

204424
ABSTRACT

A COMPUTER INTERFACED RAPID SCANNING ABSORBANCE
AND FLUORESCENCE STOPPED-FLOW SYSTEM AND ITS
APPLICATION TO THE KINETICS OF BIOLOGICAL REACTIONS

BY

GUAN-HUEI HO

A computer interfaced, double-beam, thermostated stopped-flow system for fixed wavelength and rapid scanning of absorbance or light emission (fluorescence, luminescence and reflectance) spectra has been constructed. The entire system was constructed such that the solutions contact only Pyrex, Teflon, Kel-F, polypropylene and quartz. A specially designed all quartz, double 4-jet mixing and observation cell (2 mm ID) with two optical path lengths has been made. The syringes were made out of heavy-walled Pyrex precision bore tubing (0.396" ID). Steel plungers with easily adjustable Teflon cap seals were made to fit them. Two metal flags mounted on the stopping plunger provide timing pulses by interrupting two light beams which are detected by separate phototransistors. The thermostat bath, which was made of Plexiglas to provide good visibility, surrounds the flow system and allows for temperature-dependent studies and for establishing thermal equilibrium between the solutions and the system. A rapid scanning monochromator is used to disperse either the excitation or the emission beam. In the

absorbance mode, light beams are transmitted via quartz fiber optics to both the sample cell and the reference cell, and then to a pair of photomultipliers. The emitted light (or reflected light), which is observed at 90° to the excitation beam at the short path length, is conducted with a separate quartz fiber bundle from the sample cell to the monochromator and then to a photomultiplier. Sample and reference photocurrents are converted to absorbance by use of a log ratio operational amplifier, or into partially corrected fluorescence by means of a ratio operational amplifier. The absorbance or the fluorescence analog signal is sampled and digitized at a nominal rate of 20.4 KHz, which is synchronized to the rotation of the monochromator mirror with the aid of a phase-locked-loop circuit. The signal is transmitted to a remote PDP-8/I computer for data acquisition and processing. The entire system was tested extensively by studying several well-characterized fast reactions. Its performance characteristics are excellent. The dead volume was estimated to be 60 μ l for the short path length and 146 μ l for the long path length, which resulted in dead times of 2.5 msec. and 6.5 msec., respectively, under a pushing pressure of ~ 50 psig. This instrument is especially suited to kinetics studies when only small volumes of the reagents are available. At least 6 good pushes can be obtained from only 5 ml of each reagent.

Scanning absorbance experiments on the redox reaction of chromic acid and hydrogen peroxide in acidic solutions

were carried out at 22°C. The observed first-order rate constants and the the calculated third-order rate constants were computed and were found to be in good agreement with published values.

The computer simulation of complex enzyme-catalyzed reactions has been explored. Five hysteretic enzyme models were investigated by numerically simulating the full time course of the reaction progress curve. The Bates and Frieden Model(D. B. Bates and C. J. Frieden, J. Biol. Chem., 248, 7878 (1973)) gives kinetically hysteretic behavior but does not show allosteric behavior in the saturation of enzyme activity. The Fit-Induced Model and the Monod-Wyman-Changeux (MWC) Model(with $n=2$) both show kinetically hysteretic response as well as allosteric saturation in the enzyme activity. Slow conformational changes give hysteresis in the time response of the reaction, while substrate binding at a second site causes the allostery in the enzyme activity. The cases with " zero cooperativity " and with " negative cooperativity " for the MWC Model(with $n=2$) were also simulated. The concept that an enzyme may have primitive Michaelis-Menten activity together with conformational-change-regulated Michaelis-Menten activity has been developed and the dependence of the full time course of the reaction on the initial substrate concentration and on the total enzyme concentration was also numerically simulated.

The new instrument was first used to scan the kinetics of firefly luciferase catalyzed reactions. Both the decay of

luciferin and the growth of enzyme-bound oxyluciferin occur in at least two steps, each of which is first-order. A transient intermediate absorption band was observed between ~ 420 nm and ~ 440 nm. A pseudo-isosbestic point was observed at ~ 353 nm.

The binding reactions of 1-anilino-8-naphthalene sulfonate and bovine serum albumin were scanned by measuring the fluorescence changes. At least two steps are present in the mechanism: an unobservably fast association process (the quenching of BSA fluorescence) and a slower first-order process (the enhancement of ANS fluorescence). Both processes increase the fluorescence of ANS. The first-order process shows dependence on the ratio of the equivalent concentrations, $(\text{ANS})_0/5(\text{BSA})_0$, with a decrease in the first order rate constant as the equivalent concentration ratio is increased.

The first scanning fluorescence experiments with an enzyme were done with a reaction catalyzed by lactate dehydrogenase. The reaction was followed in both directions by observing the changes in the NADH fluorescence.

The final scanning experiments were done with AMP aminohydrolase catalyzed reactions by scanning the absorbance from ~ 257 nm to ~ 300 nm. The full time course of the reactions for various concentrations of 5'-AMP at a fixed AMP aminohydrolase concentration of 0.209 mg/ml and for various total AMP aminohydrolase concentration at a fixed 5'-AMP concentration were determined. The dependence of the

full time course on various initial substrate and enzyme concentrations shows characteristics similar to the hysteretic enzyme model - MWC Model(with $n=2$). A set of the kinetics and thermodynamic parameter values, which approximately fit the experimental data, were found and the simulated full time course behavior was compared with the corresponding experimental data.

A COMPUTER-INTERFACED RAPID SCANNING ABSORBANCE
AND FLUORESCENCE STOPPED-FLOW SYSTEM AND ITS
APPLICATION TO THE KINETICS OF BIOLOGICAL REACTIONS

By

GUAN-HUEI HO

A DISSERTATION

Submitted to

Michigan State University

in partial fulfillment of the requirements

for the degree of

DOCTOR OF PHILOSOPHY

Department of Chemistry

1976

To
Shiu-Ying and My Parents

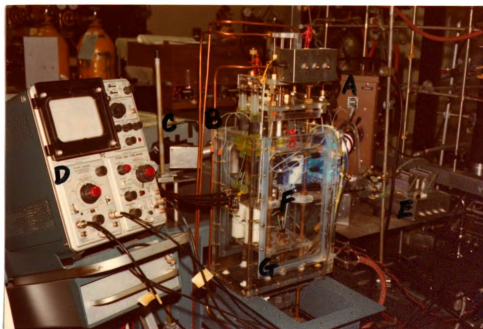
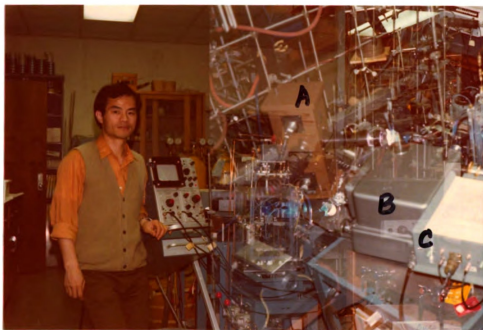
ACKNOWLEDGEMENTS

The author wishes to express his special gratitude to Professor James L. Dye for his patience, guidance, assistance and encouragement throughout the course of this work.

He would also like to thank Professor C. H. Suelter who served as my second reader for his valuable discussions, helpful suggestions and criticisms.

The author also wishes to acknowledge the cooperation of the MSU glass shop and the Chemistry Department machine shop. Thanks go to Mr. M. Rabb for his help in the trouble shooting of the interface system. Financial support from the National Science Foundation is also acknowledged.

Last, I am grateful to my wife, Shiu-Ying, for her patience and understanding which made accomplishment of this goal possible.



Author and the Rapid Scanning Absorbance and Fluorescence Stopped-Flow System. A - 1 kw Xenon lamp light source, B - rapid scanning monochromator, C - photomultiplier tube, D - storage oscilloscope, E - log ratio amplifier, F - mixing and reference cells, G - thermostat.

TABLE OF CONTENTS

	Page
LIST OF TABLES	ix
LIST OF FIGURES.	xi
PART ONE -- COMPUTER INTERFACED RAPID SCANNING ABSORBANCE AND FLUORESCENCE STOPPED-FLOW SYSTEM.	
	1
I. INTRODUCTION TO INSTRUMENTATION.	1
1.1--Rapid Scanning Spectroscopy	1
1.2--Considerations in the Instrumentation and the Computerization of Stopped- Flow System	2
1.3--Rapid Scanning Absorbance and Fluorescence Stopped-Flow Apparatus . .	4
II. THE STOPPED-FLOW SYSTEM: DESIGN, CONSTRUCTION AND TESTING.	8
2.1--Flow System Design.	10
2.2--Mixing and Reference Cells.	10
2.3--Pushing and Stopping System	17
2.3.1--Syringe and Plunger Design . . .	17
2.3.2--Mechanical System and Framework.	20
2.3.3--Stopping Syringe System.	22
2.4--Solution Delivery System.	23
2.5--Optical System Design	28
III. THE COMPUTER INTERFACED SYSTEM: DATA ACQUISITION AND PROCESSING	36
3.1--Signal Averaging Scheme	36
3.2--Signal Enhancement in Real Time	39
3.3--Determination of Maximum Sampling Rate.	39
3.4--System Control and Timing	40
3.5--System Hardware and Description	42
3.6--Remote Digital Transmission System. . .	44

	Page
3.7--Multiplication of Sampling Frequency. . .	45
3.8--System Software Description	45 ✓
3.9--System Performance.	49
3.10--Calculation Schemes Used in Data Analysis	49 ✓
IV. PERFORMANCE RESULTS.	51
4.1--Optical Calibration Data.	51
4.2--Flow Calibration.	57
4.3--Mixing Cell Performance - Fixed Wavelength Mode	59
4.3.1--Dead Time.	59
4.3.2--Mixing Efficiency and Stopping Time	61
4.3.3--Reliability of the System.	63
4.4--Quantitative Measurements - Scanning Mode.	65 ✓
4.4.1--Scanning Absorbance.	65
4.4.2--Scanning Fluorescence.	71
4.4.3--Scanning Reflectance	79
PART TWO -- COMPUTER SIMULATION OF HYSTERETIC ENZYME SYSTEMS	85
V. HYSTERETIC ENZYMES	85
5.1--Hysteresis in Enzyme Systems.	85
5.1.1--Regulation of Enzyme Catalysis	85
5.1.2--The Enzyme Models Proposed	87
5.1.2.1--MWC Model	89
5.1.2.2--AKNF Model.	90
5.1.2.3--HW Model.	92
5.1.2.4--BF Model.	92
5.2--Conformational Adaptibility and Enzymatic Catalysis.	93
VI. SIMULATION OF HYSTERETIC ENZYME SYSTEMS.	95
6.1--Computer Simulation	95
6.2--Simulation of Hysteretic Enzyme	

	Page
System	96
6.3--Hysteretic Enzyme Models	99
6.3.1--Model 1	99
6.3.2--Model 2	119
6.3.3--Model 3	136
6.3.4--Model 4	150
6.3.5--Model 5	168
6.4--Conclusions	179
PART THREE -- STOPPED-FLOW KINETICS STUDIES . . .	181
VII. RAPID SCANNING ABSORBANCE STOPPED-FLOW KINETICS	
STUDIES ON FIREFLY LUCIFERASE CATALYZED REACTIONS	181
7.1--Introduction	181
7.2--Materials and Experimental	184
7.3--Experimental Results and Preliminary	
Data Analysis.	185
7.4--Computer Fits of the Kinetics Data to	
Combined First Order Mechanisms.	189
7.4.1--Consecutive First Order Kinetics.	192 ✓
7.4.2--Parallel First Order Kinetics	193
7.5--Discussion	197
VIII. RAPID SCANNING FLUORESCENCE STOPPED-FLOW	
KINETICS STUDIES ON LACTATE DEHYDROGENASE	
CATALYZED REACTIONS	203
8.1--Introduction	203
8.2--Materials and Experimental	204
8.3--Experimental Results and Data Analysis	205
IX. RAPID SCANNING FLUORESCENCE STOPPED-FLOW KINETICS	
STUDIES ON BINDING OF 1-ANILINO-8-NAPHTHALENE TO	
BOVINE SERUM ALBUMIN.	212
9.1--Introduction	212
9.2--Materials and Experimental	213
9.3--Representative Kinetic Fluorescence	
Spectra.	214
9.4--Experimental Results and Data Analysis	220

	Page
X. RAPID SCANNING ABSORBANCE STOPPED-FLOW KINETICS STUDIES ON THE REDOX REACTION BETWEEN CHROMIC ACID AND HYDROGEN PEROXIDE	229
10.1--Introduction	229
10.2--Materials and Experimental	230
10.3--Representative Kinetic Absorbance Spectra and Time-cuts.	230
10.4--Experimental Results and Data Analysis	234
XI. RAPID SCANNING ABSORBANCE STOPPED-FLOW KINETICS STUDIES OF AMP AMINOHYDROLASE CATALYZED REACTIONS --- SUBSTRATE ACTIVATION	243
11.1--Introduction	243
11.2--Materials and Experimental	245
11.3--Experimental Results and Data Analysis	246
XII. SUGGESTIONS FOR FUTURE WORK.	260
APPENDIX 1	261
APPENDIX 2	264
APPENDIX 3	267
APPENDIX 4	271
APPENDIX 5	275
APPENDIX 6	279
APPENDIX 7	283
REFERENCES	286

LIST OF TABLES

Table	Page
2-1 Scanning monochromator and phase-locked-loop parameters. Output Sampling Frequency=20.4 KHz.	41
2-2 Flow time measurements.	61
6-1 Standard values of initial concentrations and kinetic parameters for Model 1.	103
6-2 Standard values of initial concentrations of substrate and enzyme, as well as kinetic parameters, for Model 2	123
6-3 Standard values of initial concentrations of substrate and enzyme, and each kinetic parameter, used in the simulation of Model 3. .	140
6-4 Standard values of initial concentrations of enzyme and substrate, and each kinetic parameter, for Model 4.	154
6-5 Standard values of the kinetic parameters, the initial concentration of substrate and the total enzyme concentration, for Model 5	172
7-1 First order rate constants for the luciferase catalyzed reactions(at temperature 18°C). . . .	196
7-2 First order rate constants for the luciferase catalyzed reactions(at temperature 25°C). . . .	200
9-1 Observed first order rate constants(k_{obs}) and initial ANS fluorescence intensity(F_0), obtained from computer fitting, for the binding reaction of ANS to BSA in 0.1M phosphate pH 7.0 buffer solution at $22.0 \pm 0.1^\circ\text{C}$	221
10-1 Observed pseudo-first order rate constants (k_{obs}) and calculated third-order rate constants(k), obtained from the computer fitting, for the reaction: $\text{HCrO}_4^- + 2\text{H}_2\text{O}_2 + \text{H}^+ \longrightarrow \text{CrO}_5 + 3\text{H}_2\text{O}$ (in 0.1M ionic strength at $22.0 \pm 0.1^\circ\text{C}$). . . .	238

LIST OF FIGURES

Figure		Page
2-1	Schematic diagram of the thermostated stopped-flow apparatus. A-reactant reservoirs, B-joints for reactants, C-electrically controlled 3-way pneumatic valves, D-pushing syringes, E-mixing and observation cell, F-stopping syringe, G-reference cell, H-valves, I-pneumatic cylinder, J-to vacuum and waste, K-quartz light fibers, L-thermostat bath, M-glass-to-plastic tubing connectors, N-framework.	11
2-2	Set-up for the drilling of quartz capillaries. A-Indexing head, B-From the Airbrasive unit, C-Capillary tube	13
2-3	Schematic diagram of the mixing and observation cell, A 42 cm, B 1.0 cm, C 0.5 cm, E-cross-section of a mixer	14
2-4	Set-up of cells and fiber optics. A-Fiber optics, B-Beam-splitter, C-Reference cell, D-Mixing cell.	18
2-5	Detailed view of a syringe used in the stopped-flow system. A-Teflon cap, B-threaded rod, C-Viton "O" rings, D-fill position, E-rinse position, F-locking nut.	19
2-6	Timing pulses from the flow-flags. A-start flag signal, B-flow velocity profile, C-stop flag signal, D-locations of the metal flags on the stopping plunger, E-locations of the phototransistors, F,G-data collection can be initiated at one of these points, H-constant flow velocity has been reached at this point . .	24
2-7	Timing diagram for a scanning experiment. F and B refer to forward and backward scans respectively, t_1 is called the time shift, t_2 is defined as the flow time and t_3 is the stopping time.	25
2-8	Effective Xenon lamp spectrum showing the relative PMT voltage obtained for both the forward and backward scans in a complete revolution. Output of the stopped-flow apparatus at a scanning speed of 75 spectra per second; entrance slit=0.25 mm, PMT voltage =500v, drum setting=1544, and nutation=0.64. . .	30
2-9	Absorbance circuit. A-fixed gain potentiometer,	

Figure		Page
	B-high frequency filter(controlled with toggle switches). The amplifiers are from Philbrick/Nexus Research and National Semiconductor Corporation.	34
2-10	Partially corrected fluorescence circuitry. A-fixed gain potentiometer, B-bias circuit. All the amplifiers are from National Semiconductor Corporation.	35
2-11	Example of the signal averaging scheme for a fixed wavelength case. The numbers in parentheses following the group number are the number of samples averaged into each point. The appropriate S/N values are given in the triangles	37
2-12	Computer interface for rapid scanning absorbance and fluorescence stopped-flow system	43 ✓
2-13	Flow-chart for the data acquisition routines	47
2-14	Block diagram of the computer interfaced scanning stopped-flow system --- Absorbance mode	52 ✓
2-15	Block diagram of the computer interfaced scanning stopped-flow system --- fluorescence mode.	53 ✓
2-16	Holmium oxide glass spectrum collected with the stopped-flow apparatus at a scanning rate of 13.33 msec per spectrum. The spectrum shown is the average of 100 individual spectra	54
2-17	Permanganate(in 1M H ₂ SO ₄ solution) spectrum collected with the stopped-flow apparatus at a scanning speed of 75 scans per second. The spectrum shown is the average of 100 individual spectra	55
2-18	Absorbance from the stopped-flow system <u>vs</u> absorbance from a Cary 17 spectrometer for aqueous solutions of KMnO ₄ at a wavelength of 545 nm.	56
2-19	Absorbance from the stopped-flow system <u>vs</u> absorbance from a Cary 17 spectrometer for 5'-AMP aqueous solution(in 0.05M phosphate pH 7.4 buffer solution, 22°C) at a	

Figure		Page
	wavelength of 260 nm.	58
2-20	Time-development of the FeNCS^{2+} complex at 456 nm obtained in a fixed wavelength experiment. Total times for those portions displayed are: A-1.03 sec, B-14 msec, C-9 msec, D-5.8 msec. B and C show data collection which started before the stop flag, D-shows data collection which started at the time of the stop flag.	60
2-21	Semilog plot of $(A(t_0)-A(t))/(A(t_0)-A(t_\infty))$ vs time for the dead time computation. Data obtained from the decay of the reaction at a wavelength of 352 nm.	62
2-22	Time profile of the growth of the FeNCS^{2+} complex at 456 nm, used to estimate the stopping time. The data obtained at 22°C with initial concentrations: 0.02M Fe^{3+} , 0.02M CNS^- , in 0.2M HClO_4 solution respectively.	64
2-23	Overall spectral changes for the reaction of 0.01M Fe^{3+} with 0.01M CNS^- in 0.1M HClO_4 solution at 22°C. Spectra were collected with the stopped-flow system at a scanning rate of 13.33 msec per spectrum	67
2-24	Time-cuts showing the formation of the FeNCS^{2+} ion from the reaction of Fe^{3+} with CNS^- at 22°C in 0.1M HClO_4 solution, with initial concentrations: 0.01M Fe^{3+} and 0.01M CNS^-	68
2-25	Overall spectral changes for the reaction of FeNCS^{2+} and Ce(IV) in 0.7M HClO_4 solution at 22°C. Spectra were collected with the stopped stopped-flow system at a scanning rate of 13.33 msec per spectrum	69
2-26	Time courses at various wavelengths for the reaction, $\text{FeNCS}^{2+} + 4\text{Ce(IV)}$, in 0.7M HClO_4 solution at 22°C.	70
2-27	Fluorescence spectra of Fluorescein in 1 mM NaOH solution showing the concentration sensitivity of this stopped-flow system. The spectra were obtained at 22°C, slit=2.0 mm and PMT=700V. The spectrum shown is the average of 100 collected individual spectra	72
2-28	Fluorescence spectra for 10^{-6}M Fluorescein	

	in 1 mM NaOH solution showing the dependence of fluorescence intensity on the opening of slit. The spectra were obtained with this stopped-flow system at 22°C and PMT power supply 700V. Each spectrum shown is the average of 100 collected individual spectra .	73
2-29	Fluorescence spectra for 10^{-7} M Fluorescein in 1 mM NaOH solution showing the dependence of fluorescence intensity on PMT power supply voltage. The spectra were obtained with this stopped-flow system at 22°C and slit=2.0. The background has not been subtracted. Each spectrum shown is the average of 100 collected individual spectra.	74
2-30	Fluorescence spectra for various concentrations of NADH measured with this stopped-flow system at 22°C in 0.05M phosphate pH 7.4 buffer solution. Each spectrum shown is the average of 100 collected individual spectra.	75
2-31	Fluorescence intensity <u>vs</u> concentration for NADH in 0.05M phosphate pH 7.4 buffer solution at 22°C. The fluorescence intensities were measured with this stopped-flow system	76
2-32	Fluorescence spectra for various concentrations of Bovine Serum Albumin in 0.1M phosphate pH 7.0 buffer solution at 22°C. The spectra were obtained with this stopped-flow system. Each spectrum shown is the average of 100 collected individual spectra	77
2-33	Fluorescence intensity <u>vs</u> concentration for bovine serum albumin. The fluorescence intensities of BSA in 0.1M phosphate pH 7.0 buffer solution were measured with this stopped-flow system at 22°C	78
2-34	Overall spectral changes for the binding reaction of DNA and Pt(II)(thiamine)(NH ₃) ₂ in 0.3M acetate pH 5.0 buffer solution at 22°C, with initial concentrations of 0.35 mg/ml DNA and 0.4 mg/ml Pt(II). The spectra were obtained with a scanning rate of 13.33 msec per spectrum	80
2-35	Time course obtained from a fixed wavelength	

	push at 599 nm for the binding reaction of DNA and Pt(II)(thiamine)(NH ₃) ₂ in 0.3M acetate pH5.0 buffer solution at 22°C, with initial concentrations: 0.175 mg/ml DNA and 0.4 mg/ml Pt(II).	81
2-36	Time course obtained from fixed wavelength pushes at 599 nm for the binding reaction of DNA and Pt(II)(thiamine)(NH ₃) ₂ in 0.3M acetate buffer solution at 22°C, with initial concentrations: A-0.35 mg/ml DNA and 0.4 mg/ml Pt(II), B-0.175 mg/ml DNA and 0.4 mg/ml Pt(II).	82
2-37	Time course obtained from three successive fixed wavelength pushes at 599 nm for the binding reaction of DNA and Pt(II)(thiamine)(NH ₃) ₂ in 0.3M acetate buffer solution at 22°C, with initial concentrations: 0.175 mg/ml DNA and 0.4 mg/ml Pt(II). Note that the decrease in overall reflectance was due to deposition of the complex on the cell window.. . . .	84
5-1-1	Schematic representation of hyperbolic and sigmoidal binding isotherms, the effect of allosteric activators and inhibitors on the sigmoidal isotherm and negative cooperativity. The ordinate is the fraction of sites occupied, \bar{Y} , although the initial velocity of the enzymic reaction, v , also is commonly used.	88
5-1-2	Allosteric models of Monod, Wyman and Changeux(MWC), and of Adair, Koshland, Nemethy and Filmer(AKNF) for a four-subunit enzyme. The squares and circles are different conformations of the subunits, and S is the substrate	90
5-1-3	A general allosteric model(HW) for the binding of substrate, S, to a four-subunit enzyme. The squares and the circles are different conformations of the subunits. The MWC model is shown by dashed lines and the AKNF model by dotted lines. The free substrate are omitted for the sake of clarity	91
5-1-4	A hysteretic enzyme model proposed by Bates and Frieden	92
6-1-1	The BF Model, squares are less active enzyme	

Figure		Page
	forms and circles are active enzyme forms, S is substrate and P is product	100
6-1-2a	Simulated full time courses of product growth and enzyme-substrate complexes, for Model 1 .	103
6-1-2b	Simulated full time courses of product, each species of enzyme and its complex at $S_0=4200 \mu\text{M}$, for Model 1	104
6-1-2c	Simulated full time courses of product growth and free inactive enzyme at $S_0=10500 \mu\text{M}$, for Model 1	104
6-1-3	Simulated time courses for various total enzyme concentrations, for Model 1.	106
6-1-4a	Simulated time courses for various initial substrate concentrations, for Model 1	106
6-1-4b	Simulated time courses of product growth for various higher initial substrate concentrations, for Model 1	107
6-1-5	Simulated time courses of product(P) for various values of K_1 , for Model 1	109
6-1-6	Simulated time courses of product(P) for various values of K_3 , for Model 1	109
6-1-7	Simulated time courses of product(P) for various values of k_5 , for Model 1	110
6-1-8	Simulated time courses of product(P) for various values of k_2 , for Model 1	110
6-1-9	Simulated time courses of product(P) for various values of k_6 , for Model 1	111
6-1-10	Simulated time courses of product(P) for various values of k_{-6} , for Model 1.	111
6-1-11	Simulated time courses of product growth rate for various values of total enzyme concentration, for Model 1.	113
6-1-12	Simulated time courses of product growth rate for various values of initial concentration of substrate, for Model 1	113
6-1-13	Simulated time courses of product growth rate for various values of kinetic parameters, K_1 ,	

Figure		Page
	K_3 , k_2 and k_4 , for Model 1.	114
6-1-14	Simulated time courses of product growth rate for various values of kinetic parameters, k_5 , k_6 , and k_{-6} , for Model 1. . .	115
6-1-15	Simulated time courses of product growth for various total enzyme concentrations, for Model 1	116
6-1-16	Simulated saturation curve of enzyme activity at an enzyme concentration of $0.044 \mu\text{M}$, for Model 1. For curve A, $K_1=25,000 \mu\text{M}$ and $k_2=7.5 \text{ sec}^{-1}$, for curve B, $K_1=5000 \mu\text{M}$, $k_2=80 \text{ sec}^{-1}$.	116
6-1-17	Simulated saturation curve of enzyme activity for an enzyme concentration of $0.044 \mu\text{M}$, for Model 1, with the parameter values of Frieden	117
6-1-18	Lineweaver-Burk plot, for Model 1. The values of V_0 and S_0 were obtained from Curve A of Figure 6-1-16. The Michaelis constant and V_{max} were found to be $K_m=2189 \pm 77 \mu\text{M}$ and $V_{\text{max}}=21.6 \pm 0.5 \mu\text{M/sec}$ at $(E)_0=0.044 \mu\text{M}$, respectively.	118
6-2-1	Fit-induced hysteretic enzyme model. The enzyme has one effector site and one substrate site.	120
6-2-2	Fit-induced hysteretic enzyme model	122
6-2-3	Simulated time courses of product growth and intermediates, for Model 2.	123
6-2-4	Simulated time courses of active form enzyme-effector complex for various total enzyme concentrations, for Model 2	125
6-2-5	Simulated time courses of enzyme-effector-substrate complex for various total enzyme concentrations, for Model 2	125
6-2-6	Simulated time courses of product growth for various total enzyme concentrations, for Model 2	126
6-2-7	Simulated time courses of product growth for various initial substrate concentrations, for Model 2	126
6-2-8	Simulated time courses of product growth for	

Figure		Page
	various values of K_1 , for Model 2	128
6-2-9	Simulated time courses of product growth for various values of K_3 , for Model 2	128
6-2-10	Simulated time courses of product growth for various values of k_2 , for Model 2	129
6-2-11	Simulated time courses of product growth for various values of K_4 , for Model 2	129
6-2-12	Simulated time courses of product growth for various values of k_{-6} , for Model 2.	130
6-2-13	Simulated time courses of product growth for various values of k_6 , for Model 2	130
6-2-14	Simulated time courses of product growth for various values of k_5 , for Model 2	131
6-2-15	Simulated time courses of product growth for various total enzyme concentrations, for Model 2, using ($E_0 \cdot \text{time}$) as time scale. . . .	131
6-2-16	Simulated time courses of product growth rate for various total enzyme concentrations, for Model 2	132
6-2-17	Simulated time courses of product growth rate for various initial substrate concentrations, for Model 2	132
6-2-18	Simulated time courses of product growth rate for various values of K_1 , k_2 , K_3 and K_4 , for Model 2	133
6-2-19	Simulated time courses of product growth rate for various values of k_5 , k_6 and k_{-6} , for Model 2	134
6-2-20	Simulated saturation curve of enzyme activity at an enzyme concentration of 0.044 μM , for Model 2	135
6-3-1	Compound hysteretic enzyme model for one subunit with one effector site and one catalytic site. Circle is catalytic site and half circle is effector site.	137
6-3-2	Compound hysteretic enzyme model for one subunit with one effector site and one catalytic site.	138

Figure		Page
6-3-3a	Simulated time courses of product growth, each form of free enzymes, and the intermediates, for Model 3	140
6-3-3b	Simulated time courses of product growth, each form of free enzyme and its complex with $K_4=K_7$ and $k_5=k_8$, for Model 3.	141
6-3-3c	Simulated time courses of product growth and inactive form free enzyme with $K_4=K_7$ and $k_5=k_8$ at $S_0=2100 \mu\text{M}$, for Model 3	141
6-3-4	Simulated time courses of product growth for various total enzyme concentrations, for Model 3.	143
6-3-5	Simulated time courses of product growth for various initial substrate concentrations, for Model 3.	143
6-3-4b	Simulated time courses of product growth for various total enzyme concentrations with $K_4=K_7$ and $k_5=k_8$, for Model 3	144
6-3-5b	Simulated time courses of product growth for various initial substrate concentrations with $K_4=K_7$ and $k_5=k_8$, for Model 3.	144
6-3-6	Simulated time courses of product growth for various values of K_1 , for Model 3.	145
6-3-7	Simulated time courses of product growth for various values of K_3 , for Model 3.	145
6-3-8	Simulated time courses of product growth for various values of k_2 , for Model 3.	146
6-3-9	Simulated time courses of product growth for various values of k_6 , for Model 3.	146
6-3-10	Simulated time courses of product growth for various values of K_4 , for Model 3.	147
6-3-11	Simulated time courses of product growth for various values of K_7 , for Model 3.	147
6-3-12	Simulated time courses of product growth for various values of k_5 , for Model 3.	148
6-3-13	Simulated time courses of product growth for various values of k_8 , for Model 3.	148

Figure		Page
6-3-14	Simulated time courses of product growth for various values of k_{-6} , for Model 3	149
6-3-15	Simulated saturation curve of enzyme activity for an enzyme concentration of $0.044 \mu\text{M}$, for Model 3.	149
6-4-1	Two subunit, symmetric and concerted, hysteretic enzyme model.	151
6-4-2	Two subunit, symmetric and concerted, hysteretic enzyme model. This is the case of MWC model with $n=2$	153
6-4-3a	Simulated full time courses of product(P) growth, inactive form free enzyme(E) and active form enzyme-substrate($E_{s2}^!$), for Model 4.	154
6-4-3b	Simulated full time courses of product growth, free enzymes and their complexes with $k_9=k_{11}$, for Model 4.	155
6-4-3c	Simulated full time courses of product growth, inactive form enzyme(E) and enzyme complex($E_{s2}^!$), with $k_9=k_{11}$ at $S_0=1260 \mu\text{M}$, for Model 4.	155
6-4-4a	Simulated time courses of product growth for various total enzyme concentrations, for Model 4.	157
6-4-5a	Simulated time courses of product growth for various initial substrate concentrations, for Model 4.	157
6-4-4b	Simulated time courses of product growth for various total enzyme concentrations with $k_9=k_{11}$, for Model 4.	158
6-4-5b	Simulated time courses of product growth for various initial substrate concentrations with $k_9=k_{11}$, for Model 4.	158
6-4-4c	Simulated time courses of product growth for various total enzyme concentrations with $k_9=k_{11}$, for Model 4, using $(E_0 \cdot \text{time})$ as time scale	159
6-4-6	Simulated time courses of product growth for various values of K_1 , for Model 4.	161

Figure		Page
6-4-7	Simulated time courses of product growth for various values of K_5 , for Model 4	161
6-4-8	Simulated time courses of product growth for various values of k_2 , for Model 4	162
6-4-9	Simulated time courses of product growth for various values of k_9 , for Model 4.	162
6-4-10	Simulated saturation curve of enzyme activity at an enzyme concentration of $0.044 \mu\text{M}$, for Model 4.	163
6-4-11a	Simulated time courses of product growth for various total enzyme concentrations, with $K_1=1250 \mu\text{M}$, $K_3=5000 \mu\text{M}$, $K_5=50 \mu\text{M}$ and $K_7=200 \mu\text{M}$, for Model 4.	164
6-4-11b	Simulated time courses of product growth for various initial substrate concentrations, with $K_1=1250 \mu\text{M}$, $K_3=5000 \mu\text{M}$, $K_5=50 \mu\text{M}$ and $K_7=200 \mu\text{M}$, for Model 4	164
6-4-12a	Simulated time courses of product growth for various total enzyme concentrations, with $K_1=5000 \mu\text{M}$, $K_3=10,000 \mu\text{M}$, $K_5=200 \mu\text{M}$ and $K_7=400 \mu\text{M}$, for Model 4	165
6-4-12b	Simulated time courses of product growth for various initial substrate concentrations, with $K_1=5000 \mu\text{M}$, $K_3=10,000 \mu\text{M}$, $K_5=200 \mu\text{M}$ and $K_7=400 \mu\text{M}$, for Model 4	165
6-4-13	Simulated saturation curves of enzyme activity at an enzyme concentration of $0.044 \mu\text{M}$, for Model 4. For curve A, using the same parameter values of Figure 6-4-11, for curve B, using the same parameter values of Figure 6-4-12 . .	166
6-5-1	Two subunit compound hysteretic enzyme model. Squares are inactive states and the circles are active states of the enzyme.	168
6-5-2	Two subunit compound hysteretic enzyme model .	169
6-5-3	Simulated time courses of product growth, the growth-and-decay of each of the free enzymes	

	and the enzyme-substrate complexes, for Model 5.	171
6-5-4	Simulated time courses of product growth for various total enzyme concentrations, for Model 5.	173
6-5-5	Simulated time courses of product growth for various initial substrate concentrations for Model 5.	173
6-5-6	Simulated time courses of product growth for various values of K_1 , for Model 5.	174
6-5-7	Simulated time courses of product growth for various values of k_9 , for Model 5.	174
6-5-8	Simulated time courses of product growth for various values of k_{10} , for Model 5.	175
6-5-9	Simulated time courses of product growth for various values of k_{11} , for Model 5.	175
6-5-10	Simulated time courses of product growth for various values of k_{10} , including $k_{10}=0$, for Model 5.	176
6-5-11	Simulated saturation curve of enzyme activity at an enzyme concentration of $0.044 \mu\text{M}$, for Model 5.	177
6-6-1	Simulated saturation curves of enzyme activity for Model 1 through Model 5 at $(E)_0=0.044 \mu\text{M}$	179
7-1	Components in the luciferase catalyzed reactio reactions.	182
7-2	Overall spectral changes for the firefly luciferase catalyzed reaction in 0.025M glycylglycine pH 7.8 buffer solution at $25 \pm 0.1^\circ\text{C}$. The initial concentrations are: $16.1 \mu\text{M}$ luciferin with 1 mM ATP and 2.5 mM Mg^{++} , and $4 \mu\text{M}$ luciferase.	186
7-3	Time cuts showing the decay of substrate(LH_2), the growth of enzyme-bound product and the growth-decay of the transient intermediate for the firefly luciferase catalyzed reactions in 0.025M glycylglycine pH 7.8 buffer solution at $25 \pm 0.1^\circ\text{C}$	187

Figure		Page
7-4	Time course for the transient intermediate(s) in the early 23 sec for the luciferase catalyzed reaction in 0.025M glycylglycine pH 7.8 buffer solution at $25.0 \pm 0.1^\circ\text{C}$	188
7-5	Semilog plot of $(A(t)-A(t_\infty))/(A(t_0)-A(t_\infty))$ vs time for the luciferase catalyzed reaction. The data obtained from Figure 7-3.	190
7-6	Semilog plot of $(A(t_\infty)-A(t))/(A(t_\infty)-A(t_0))$ vs time for the luciferase catalyzed reaction. The data obtained from Figure 7-3.	191
7-7	Postulated sequence of events for luciferase catalyzed reactions.	189
7-8	Computer fits for LH_2 decay at various wav wavelengths in the luciferase catalyzed reaction, with the assumption of a consecutive first order mechanism.	194
7-9	Computer fits for enzyme-bound product growth at various wavelengths in the luciferase catalyzed reaction, with the assumption of a consecutive first order mechanism.	195
7-10	Computer fits for LH_2 decay at various wavelengths in the luciferase catalyzed reaction, with the assumption of a parallel first order mechanism.	198
7-11	Computer fits for the enzyme-bound product growth at various wavelengths in the luciferase catalyzed reaction, with the assumption of a parallel first order mechanism	199
8-1	The overall kinetic fluorescence spectra for the backward reaction in 0.05M phosphate pH 7.4 buffer solution at $22.0 \pm 0.1^\circ\text{C}$. Solvent background has been subtracted	206
8-2	Characteristic spectra isolated from Figure 8-1, showing the red shift of the fluorescence maximum of bound NADH during the reaction	207
8-3	Time cuts of Figure 8-1, showing the decay of NADH during the first 3.6 sec of reaction, at various wavelengths.	208

8-4	The isolated kinetic fluorescence spectra for the forward reaction in 0.05M phosphate pH 7.4 buffer solution at $22.0 \pm 0.1^\circ\text{C}$. Solvent background has not been subtracted	209
8-5	Time cuts of Figure 8-4, showing the growth of NADH, at various wavelengths.	210
9-1	Overall spectral changes for the ANS-BSA binding reaction in 0.1M phosphate pH 7.0 buffer solution at 22°C . The initial concentrations are: $15\ \mu\text{M}$ ANS and $3.8\ \mu\text{M}$ BSA. The spectra were obtained with a scanning rate of 13.33 msec. per spectrum	215
9-2	Overall spectral changes for the ANS-BSA binding reaction in 0.1M phosphate pH 7.0 buffer solution at $22.0 \pm 0.1^\circ\text{C}$	216
9-3	Overall fluorescence spectral changes for two different BSA concentrations in 0.1M phosphate pH 7.0 buffer solution at $22.0 \pm 0.1^\circ\text{C}$	217
9-4	Time development of ANS fluorescence enhancement for the ANS-BSA binding reaction with initial concentrations: $15\ \mu\text{M}$ ANS and $3.8\ \mu\text{M}$ BSA, in 0.1M phosphate pH 7.0 buffer solution at 22°C . The spectra were obtained from a fixed wavelength experiment at 524 nm for three successive pushes.	218
9-5	Time courses showing two successive fixed wavelength pushes at 359 nm for the ANS-BSA binding reaction in 0.1M phosphate pH 7.0 buffer solution at 22°C , with initial concentrations: $5\ \mu\text{M}$ ANS and $3.8\ \mu\text{M}$	219
9-6a	Initial and final fluorescence intensities obtained at $(\text{ANS})_0 = 15\ \mu\text{M}$, for the ANS-BSA binding reaction in 0.1M phosphate pH 7.0 buffer solution at 22°C	223
9-6b	Plot of the observed first order rate constants (k_{obs}) vs the ratio of the equivalent initial concentrations, $(\text{ANS})_0/5(\text{BSA})_0$, for the binding reaction of ANS to BSA in 0.1M phosphate	

	pH 7.0 buffer solution at $22.0 \pm 0.1^\circ\text{C}$	224
9-7a	Computer fits for the binding reaction of ANS to BSA in 0.1M phosphate pH 7.0 buffer solution at $22.0 \pm 0.1^\circ\text{C}$, for $(\text{BSA})_0 = 3.8 \mu\text{M}$. The concentration of ANS is $5 \mu\text{M}$	225
9-7b	Computer fits for the binding reactions of ANS to BSA in 0.1M phosphate pH 7.0 buffer solution at $22.0 \pm 0.1^\circ\text{C}$, for $(\text{BSA})_0 = 5 \mu\text{M}$ and $10 \mu\text{M}$. The initial concentration of ANS is $5 \mu\text{M}$	226
9-8a	Computer fit for the binding reaction of ANS to BSA in 0.1M phosphate pH 7.0 buffer solution at $22.0 \pm 0.1^\circ\text{C}$, for $(\text{BSA})_0 = 3.8 \mu\text{M}$. The initial concentration of ANS is $15 \mu\text{M}$	227
9-8b	Computer fits for the binding reaction of ANS to BSA in 0.1M phosphate pH 7.0 buffer solution at $22.0 \pm 0.1^\circ\text{C}$, for $(\text{BSA})_0 = 5 \mu\text{M}$ and $10 \mu\text{M}$. The initial concentration of ANS is $15 \mu\text{M}$	228
10-1	Overall kinetic absorbance spectra for the redox reaction of chromic acid and hydrogen peroxide. The reaction was carried out in 0.1M ionic strength at $22.0 \pm 0.1^\circ\text{C}$, and was observed with a path length of 2 mm. The spectra were collected with a scanning rate of 13.33 msec/spectrum.	231
10-2	Time cuts of Figure 10-1, showing the disappearance of chromic acid and the growth of peroxychromic acid (fast growth followed by a subsequent slow decomposition).	232
10-3	Time cuts for the formation of peroxychromic acid, showing the slow decomposition process observed at 576 nm at 0.1M ionic strength and $22.0 \pm 0.1^\circ\text{C}$	233
10-4	Time cuts at various wavelengths, obtained from a push of the reaction of chromic acid with hydrogen peroxide in 0.1M ionic strength at $22.0 \pm 0.1^\circ\text{C}$. The reaction was observed with a path length of 1.9 cm.	235
10-5	Plots of $\ln(A(t) - A(t_\infty))$ vs time at various wavelengths for the formation of peroxychromic acid in 0.1M ionic strength at $22.0 \pm 0.1^\circ\text{C}$	236

Figure		Page
10-6a	Computer fits for the redox reaction of chromic acid and hydrogen peroxide in 0.1M ionic strength at $22.0 \pm 0.1^\circ\text{C}$, at wavelengths 337 nm and 352 nm. The initial concentrations are: $(\text{HCrO}_4^-)_0 = 0.5 \text{ mM}$, $(\text{H}_2\text{O}_2)_0 = 7 \text{ mM}$ and $(\text{H}^+)_0 = 14 \text{ mM}$	240
10-6b	Computer fits at wavelengths 372 nm and 348 nm for the same push of Figure 10-6a. . .	241
10-6c	Computer fits at wavelengths 544 nm and 576 nm for the same push of Figure 10-6a	242
11-1	Overall kinetic absorbance spectra for the AMP deaminase catalyzed reaction in 0.05M Tris-Mes pH 6.4 buffer solution at $22.0 \pm 0.1^\circ\text{C}$	247
11-2	Some isolated intermediate spectra of Figure 11-1, collected at specific time of reaction.	248
11-3	Time cuts at various wavelengths of Figure 11-1, for the first 30 sec of the reaction.	249
11-4	Time course of the absorbance change at 287 nm from Figure 11-1, for the first 14 sec of the reaction.	251
11-5	Full time course of the AMP deaminase catalyzed reaction, showing the growth of IMP at 287 nm, in 0.05M Tris-Mes pH 6.4 buffer solution at $22.0 \pm 0.1^\circ\text{C}$	252
11-6	Time course of the AMP deaminase catalyzed reaction, showing the fraction of reaction obtained at various wavelengths from the same push, in 0.05M Tris-Mes, 0.2M TMACl, pH 6.4 buffer solution at $22.0 \pm 0.1^\circ\text{C}$	253
11-7	Time course of the AMP deaminase catalyzed reaction, showing the fraction of reaction obtained at 266 nm from two successive pushes in 0.05M Tris-Mes, 0.2M TMACl, pH 6.4 buffer solution at $22.0 \pm 0.1^\circ\text{C}$	254
11-8	Full time course of the AMP deaminase catalyzed reactions, showing the dependence of reaction progress on the initial substrate concentration, in 0.05M Tris-Mes pH 6.4 buffer solution at $22.0 \pm 0.1^\circ\text{C}$. The total enzyme	

Figure		Page
	concentration is 0.209 mg/ml	255
11-9	Full time course of the AMP deaminase catalyzed reactions, showing the dependence of the reaction progress on the total enzyme concentration, in 0.05M Tris-Mes pH 6.4 buffer solution at $22.0 \pm 0.1^\circ\text{C}$. The initial substrate concentration is 0.025 mM.	256
11-10	Comparison of the computer simulated full time course of the reaction with the experimental data in Figure 11-6.	258
11-11	Comparison of the computer simulated full time course of the reaction with the experimental data in Figure 11-7.	259